RA'EGA
O ESPAÇO GEOGRÁFICO EM ANÁLISE
https://revistas.ufpr.br/raega

ISSN eletrônico 2177-2738
RA'EGA, Curitiba, PR, V.60, n.1, p. 45 – 69, 8/2024
http://dx.doi.org/10.5380/raega.v60i0.95709

Energy Balance in Forest, Natural Field and Agricultural Area in the Municipality of Humaitá-AM

Balanço de Energia em Floresta, Campo Natural e Área Agrícola no Município de Humaitá-AM

Kim Besinge Miranda Lobato[*], Carlos Alexandre Santos Querino [**], Luiz Octávio Fabrício dos Santos[***], Juliane Kayse Albuquerque da Silva Querino[****], Rosa Maria Nascimento dos Santos[*****]

[*]Programa de Pós-graduação em Clima e Ambiente, Instituto Nacional de Pesquisas da Amazônia, kbml.mcl21@uea.edu.br
[**]Instituto de Educação Agricultura e Ambiente - IEAA, Universidade Federal do Amazonas – UFAM, carlosquerino@ufam.edu.br
[***]Programa de Pós-graduação em Física Ambiental – PPGCA, Universidade Federal de Mato Grosso – UFMT, luizoctavio@fisica.ufmt.br
[****]Programa de Pós Graduação em Ciências Ambientais, Instituto de Educação Agricultura e Ambiente - IEAA, Universidade Federal do Amazonas-UFAM, julianekayse@ufam.edu.br
[*****]*IN MEMORIAM*

http://dx.doi.org/10.5380/raega.v60i0.95709

Abstract

The climatic consequences of changes in forest areas can be assessed through the analysis of the Surface Energy Balance, through either *in situ* measurements or Remote data modeling, such as those carried out by SEBAL. Thus, this work aimed to analyze the variation in the energy balance on the surface in a farm area, natural field and forest for the region of Humaitá, AM, Brazil. The satellite data was collected in the years 2000, 2005, 2015 and 2020 and processed in geeSebal. The automatic calibration technique was performed to identify the hot and cold pixels. The energy balance variables were estimated using the simplified version of the Calibration Using Inverse Modeling at Extreme Conditions algorithm, developed for the METRIC model and applicable to the SEBAL algorithm. Statistical analysis was performed using descriptive statistics, using the Kruskal-Wallis test and Dunn's post-hoc test. The results showed that soil heat flux and sensible heat flux were lower in forests and higher in fields and farms. The latent heat flux and net radiation assumed the highest values in forests and lowest in fields and farms. The post-hoc Dunn test showed a similarity between the fields and farm areas. Finally, the SEBAL model satisfactorily estimated the components of the energy balance at the surface, in addition to highlighting the increase in sensible heat and the decrease in latent heat for the study areas.

Keywords:
Energy fluxes, SEBAL, Climate, Remote Sensing.

Resumo

As consequências climáticas das alterações de áreas de florestas podem ser avaliadas através da análise do Balanço de Energia em Superfície, seja por medidas *in loco* ou modelagem de dados remoto, como as realizadas pelo SEBAL. Assim, este trabalho teve como objetivo analisar a variação

ISSN eletrônico 2177-2738
RA'EGA, Curitiba, PR, V.60, n.1, p. 45 – 69, 8/2024
http://dx.doi.org/10.5380/raega.v60i0.95709

do balanço de energia na superfície em área de fazenda, campo natural e floresta para a região de Humaitá, AM, Brasil. Os dados de satélite foram coletados nos anos de 2000, 2005, 2015 e 2020 e processados no *geeSebal*. A técnica de calibração automática foi utilizada para identificar os pixels quente e frio. As variáveis do balanço de energia foram estimadas através da versão simplificada do algoritmo *Calibration Using Inverse Modeling at Extreme Conditions*, desenvolvido para o modelo METRIC e aplicável ao algoritmo SEBAL. A análise estatística foi realizada através da estatística descritiva, por meio do teste Kruskal-Wallis e o teste *post-hoc* de Dunn. Os resultados mostraram que o fluxo de calor no solo e o fluxo de calor sensível foi menor em floresta e maiores em campos e fazenda. O fluxo de calor latente e o saldo de Radiação assumiu os maiores valores em floresta e menores em campos e fazenda. O teste *post-hoc* Dunn mostrou uma semelhança entre as áreas de campos e fazenda. Por fim, o modelo SEBAL estimou de maneira satisfatória os componentes do balanço de energia na superfície, além de evidenciar o aumento do calor sensível e a diminuição do calor latente para as áreas de estudo.

Palavras-chave:
Fluxos energéticos, SEBAL, Clima, Sensoriamento Remoto.

I. INTRODUCTION

The Amazon Forest is the largest tropical forest in the world, and it is important for climate control at different scales, since this biome maintains water cycling and carbon storage (MARQUES et al., 2017). Most of the Amazon is in the state of Amazonas, which is divided into four mesoregions: North, Southwest, Middle and South of Amazonas (IBGE, 2017). Even with its climatic importance influence and rich biodiversity, the Amazon Forest, in recent decades, has been undergoing structural changes, mainly due to human activities, such as changes from forest areas to managed areas, agricultural lands and pastures (ROTHMUND et al., 2019). These changes in surface use and coverage are most noticeable in the southern mesoregion of the state.

The Southern Amazonian mesoregion is responsible for a large part of the agricultural production in the state of Amazonas (IDAM, 2018). The incentive to increase cultivation areas was due to a set of factors such as: low land prices, reduction in transport tariffs, relief from taxes on soy and its derivatives, among others (LIMA, 2008). With the incentives, the municipality of Humaitá was the main producer of the Madeira Complex. Soybean production in the region, for the year 2017, was 500 hectares, with total productivity of 1.3 tons. In the 2019/2020 harvest, there was an increase in the plantation area to 2 thousand hectares, and a jump to around 6 tons in production (IDAM, 2020). As a result, there was an increase in the agricultural and timber area, which caused the highest deforestation rates in the entire state being in this mesoregion, which is also located in the region known as the "deforestation arc" (PAVÃO et al., 2014).

ISSN eletrônico 2177-2738
RA'EGA, Curitiba, PR, V.60, n.1, p. 45 – 69, 8/2024
http://dx.doi.org/10.5380/raega.v60i0.95709

These increases in the agricultural and timber areas result in an impact on land cover (ANDRADE et al., 2021). Therefore, changes in the land cover modify the transfer of water vapor to the atmosphere, alter the radiation balance and, consequently, the surface energy balance (BIUDES et al., 2015; MACHADO et al., 2017). Changes in the energy balance at the surface modifies the hydrological cycle and climate variables (MARQUES et al., 2017).

However, there are a few studies that show the impacts of the natural surface cover replacement into agricultural cultivation areas in the southern mesoregion of Amazonas on the climatic variables patterns (PAVÃO et al., 2017). One of the ways to evaluate agricultural impacts is through the analysis of the surface energy balance, once changes in land cover tend to modify the surface albedo, the balance of short and long waves and, consequently, the energy balance at the surface (QUERINO et al., 2006; BIUDES et al., 2015; QUERINO et al., 2017; QUERINO et al., 2020). However, due to the lack of micrometeorological towers in the region, to monitor fluxes to estimate the energy balance *in situ*, it is necessary to use alternative means and techniques such as remote sensing.

The remote sensing technique, using multispectral and thermal images in the algorithms, becomes extremely important, once it allows estimating the energy balance on the surface based on data from orbital satellites, which do not require much meteorological data and generate reliable estimates to regional and local scale (ZHANG et al., 2016; CHEN et al., 2020). For Chang et al. (2017), most of these estimates are based on an one-dimensional fluxes model that describes the mechanisms of radiation exchange and heat fluxes that occur between the surface and the atmosphere, following the principle of energy conservation. Among the most used models, the Surface to Earth Energy Balance Model (SEBAL) (BASTIAANSSEN et al., 1998) has been successfully applied in different climatic regions and in different land covers (BASTIAANSSEN et al., 2005; RUHOFF et al., 2012; TANG et al., 2013; WAGLE et al., 2017).

Thus, this paper aimed to analyze, using the SEBAL model, the spatial-temporal variation of the surface energy balance in soybean cultivation, natural field and dense forest areas for the municipality of Humaitá, in the southern region of the Amazonas state.

II. Material and Methods

Study Area

The study has been carried out in three areas of approximately 20 km² each, with distinct physiological characteristics: Forest, Natural Field, Agricultural Area (farm intended for soybean plantation) (Figure 1). The

ISSN eletrônico 2177-2738
RA'EGA, Curitiba, PR, V.60, n.1, p. 45 – 69, 8/2024
http://dx.doi.org/10.5380/raega.v60i0.95709

areas are placed in the municipality of Humaitá, located in the southern region of the Amazonas state (Lat.: 7° 30′ 22″ S and Long.: 63° 1′ 38″ W). The municipality is located in a region of open forests and complexes of fields, known as "Campos Naturais" (natural fields), where there is a predominance of grasses and low mesophilic forests, tall evergreen forests, palm trees, chestnut groves, among others (VIDOTTO et al., 2007).

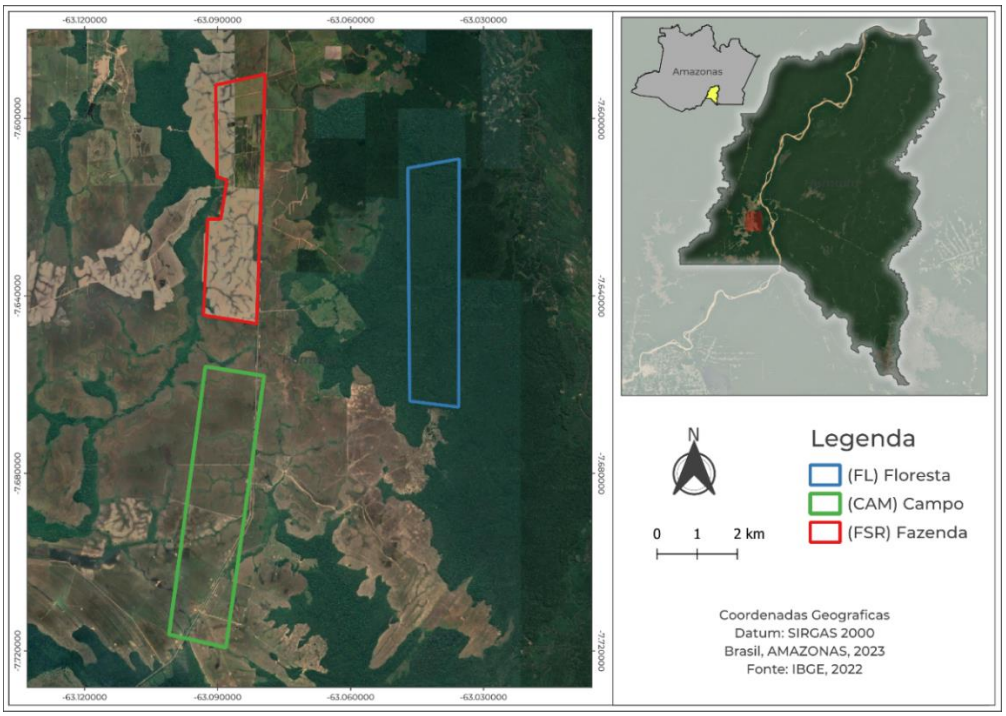

Figure 1 – Location of the municipality of Humaitá in the state of Amazonas and the areas of Forest (FL), Field (CAM) and Farm (FSR), selected for the study. Source: Own authorship using image from Google Earth.

The region's climate, according to Köppen's classification, is tropical humid (Am), and according to the more detailed classification of Thornthwaite and Mather, it is humid with moderate water deficiency in winter (B4WA'a') (MARTINS et al., 2023). According to the same authors, the average air temperature varies between 25 and 27 °C, with maximums of 36 °C and minimums that can eventually reach 17 °C during cold periods. The monthly average relative humidity varies between 85 and 90%, reaching 50% during the dry season. The wet period occurs from October to April, with total averaged rainfall of approximately 300 mm month^{-1}, while the dry period, between the months of June and August, has total average rainfall of 50 mm month^{-1}. The months of May and September correspond to the wet-dry transition period and the dry-wet transition, respectively (PEDREIRA JUNIOR et al., 2018).

Reanalysis Data

Precipitation data from the ERA5-LAND reanalysis product, made available by the European Center for Medium-Range Weather Forecasts ECMWF, were used to calculate the climatological normal (30 years, 1991 –

ISSN eletrônico 2177-2738
RA'EGA, Curitiba, PR, V.60, n.1, p. 45 – 69, 8/2024
http://dx.doi.org/10.5380/raega.v60i0.95709

2020). The monthly totals were extracted from the same database and, subsequently, after data processing, the monthly rainfall anomalies were calculated for each year of the study.

Collect of Imageries

The used imageries were generated by the Thematic Mapper – TM sensor on the Landsat 5 satellite, for the years 2000, 2010 and 2005, and by the Operational Land Imager – OLI and Thermal Infrared Sensor – TIRS sensors on board Landsat 8 for the years 2015 and 2020 (Table 1). To avoid negative interference obtaining energy fluxes, imageries with no clouds were selected between the months of June and August (dry period in the region).

Table 1 – Description of dates, time, type, path row and orbit information of the satellites that were used to acquire the imageries.

Date	Local Time	Landsat	Path Row	Orbit
06/07/2000	09:57:07	5	232	65
04/07/2005	10:07:56	5	232	65
19/08/2010	10:10:37	5	232	65
30/06/2015	10:19:42	8	232	65
29/07/2020	10:20:15	8	232	65

Font: Metabases of the imageries downloaded on the United States Geological Survey (USGS) (https://earthexplorer.usgs.gov/)

Data Processing

Imageries processing was done by using spectral radiance, surface reflectance for Landsat 5 and 8 satellites and brightness temperature in bands 6 and 10 for Landsat 5 and Landsat 8, respectively. The red bands (Landsat 5: 0.63 – 0.69 µm; Landsat 8: 0.64 – 0.67 µm), near infrared (Landsat 5: 0.76 – 0.90 µm; Landsat 8: 0.85 – 0.88 µm) and the thermal infrared band (Landsat 5: 10.4 – 12.5 µm; Landsat 8: 10.6 – 11.19 µm) were also used.

Imageries processing and the estimation of the energy balance components were carried out by using the SEBAL model, which was processed using free software: QGIS version 3.28.2 and Python 3.10. In QGIS, the study regions have been cut and, later, the steps adopted by the SEBAL model were modeled, the pixels extractions, the statistical analyzes and the figures were performed in Python.

- *The Surface Energy Balance Algorithm for Land (SEBAL)*

The SEBAL algorithm uses multispectral remote sensing data that, associated with meteorological data, can estimate the instantaneous components of the energy balance at the surface (RUHOFF et al., 2012).

ISSN eletrônico 2177-2738
RA'EGA, Curitiba, PR, V.60, n.1, p. 45 – 69, 8/2024
http://dx.doi.org/10.5380/raega.v60i0.95709

Using the surface energy balance equation (Equation 1), SEBAL estimates LE as a residue of the other components (Equation 2) (LAIPELT et al., 2020).

$$N_R = H + LE + G \quad \text{(Equation 1)}$$

$$LE = R_N - H - G \quad \text{(Equation 2)}$$

Where all components of Equation 1 being given in W m^{-2}, H is the sensible heat flux (Equation 3), N_R is the net radiation (Equation 4) and G is the soil heat flux (Equation 5) (BASTIAANSSEN, 2000):

$$H = \frac{\rho_a C_p dT}{r_{ah}} \quad \text{(Equation 3)}$$

$$N_R = (1-\alpha)R_{SW\downarrow} + R_{LW\downarrow} - R_{LW\uparrow} - (1-\varepsilon_0)R_{LW\downarrow} \quad \text{(Equation 4)}$$

$$\frac{G}{N_R} = \alpha(T_s - 273{,}15)(0{,}0038\alpha + 0{,}0074\alpha^2)(1 - 0{,}98NDVI^4) \quad \text{(Equation 5)}$$

with α, being the surface albedo, ε_0 the surface emissivity, and T_s the surface temperature (Equation 6) (ALLEN et al., 2007):

$$T_s = \frac{Tb}{1+\left(\frac{\delta Tb}{1{,}438e^{-2}}\right)\log(\varepsilon_{NB})} \quad \text{(Equation 6)}$$

in which *Tb* is the brightness temperature band (K), δ is the wavelength (μm) and ε_{NB} is the surface emissivity for the thermal band that was used. T_s was adapted to a standard elevation considering the Shuttle Radar Topography Mission (SRTM) digital elevation product, with a variation rate of 0.0065 °C^{-1} (LAIPELT et al., 2020).

Since *H* and the aerodynamic resistance for turbulent heat transport (r_{ah}) are unknown, H (Equation 3) is estimated using an iterative method. In Equation 3 we have, C_p being the specific thermal capacity, r_{ah} is the aerodynamic resistance to turbulent heat transport from the evaporation surface at height z_1 to the air above the evaporation surface z_2 (LAIPELT et al., 2021). If *H*=0, then *LE* corresponds to all available energy (BASTIAANSSEN et al., 1998a).

- *geeSebal*

geeSEBAL was developed within GEE (version 0.1.217) through the JavaScript and Python APIs (version 3.6 or higher). The SEBAL algorithm was implemented in GEE (geeSEBAL - version 0.1.217) using the JavaScript and Python APIs (Laipelt et al., 2021). GEE provides the entire Landsat collection and hourly ERA5-Land meteorological data, allowing geeSEBAL processing to be applied in different regions of the globe with high-

ISSN eletrônico 2177-2738
RA'EGA, Curitiba, PR, V.60, n.1, p. 45 – 69, 8/2024
http://dx.doi.org/10.5380/raega.v60i0.95709

performance computing, even in regions where terrestrial meteorological data is completely limited (GONÇALVES et al., 2022).

Laipelt et al. (2021), describes that geeSebal has three main considered functions: i) Image: ET estimation of a specific image (JavaScript and Python); ii) Image Collection: batch process that improves the ET estimate for a given period (exclusive to Python); iii) Time Series: ET time series estimates for longer periods according to coordinates provided by the user (exclusive to Python).

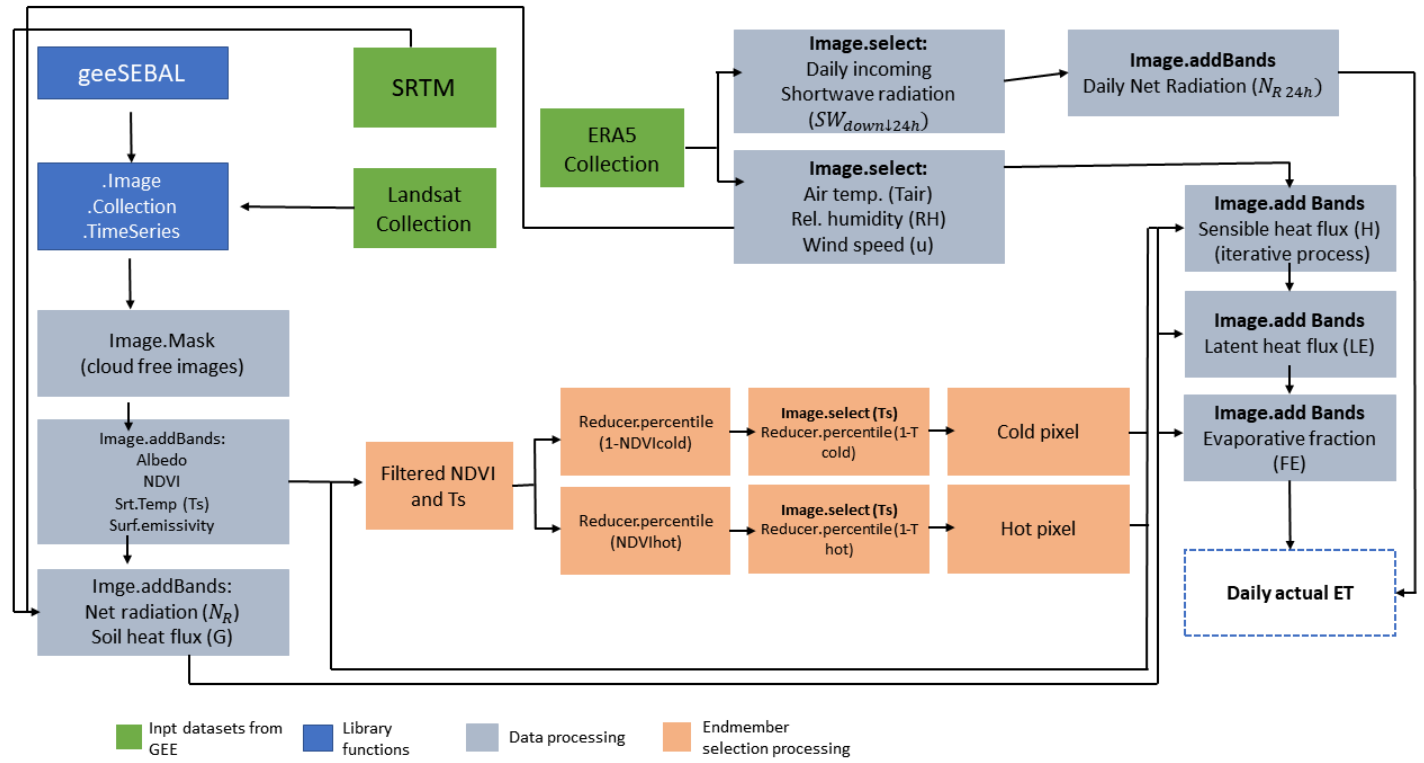

Figure 2 - Geesebal's workflow, demonstrating remote sensing data and input weather data, as well as GHE data processing functions to estimate daily evapotranspiration. (Source: Laipelt et al., 2021)

Automatic Calibration

The automatic calibration technique has been used to identify hot and cold pixels and is based on a simplified version of the Calibration Using Inverse Modeling at Extreme Conditions (CIMEC) algorithm, which was developed for the Metric model being applicable to the SEBAL Algorithm (ALLEN et al., 2013). CIMEC employs percentis of Ts and $NDVI$ for the selection. The cold pixel is defined as the one randomly chosen within the set of candidate pixels that have the highest values of $NDVI$ (5%) and, among these, the lowest values of Ts (20%). On the other hand, the hot pixel is identified by selecting 10% lower values of $NDVI$ and 20% higher values of Ts.

ISSN eletrônico 2177-2738
RA'EGA, Curitiba, PR, V.60, n.1, p. 45 – 69, 8/2024
http://dx.doi.org/10.5380/raega.v60i0.95709

In the context of the implemented model on Google Earth Engine (GEE) and the Python library, these percentiles were configured by default. However, users have the flexibility to adjust these values to achieve the most accurate results. Thus, for each region of the study area, a group of optimized percentiles based on the variation of the original CIMEC percentiles was manually selected. In this study, the Landsat scene covers the three areas of the study, the arithmetic average of percentile groups was calculated to smooth the impact on the selection of the hot and cold pixels. In this scenario, percentile groups were used as described by Laipelt et al. (2020; 2021) in regions with the same land coverage (Table 2).

Table 2 - Percentile group used for the arithmetic average for the selection of hot and cold pixels in the study area.

	Forest	Natural Field	Farm	Average
$NDVI_{cold}$	5	5	5	5
Ts_{cold}	0.01	1	1	0,67
$NDVI_{hot}$	10	1	1	4
Ts_{hot}	0.01	10	10	6,67

Font: Laipelt et al. (2020; 2021). Adapted by the authors.

Data Analysis

The Kruskal-Wallis test was created by William Kruskal (1919-2005), American mathematician and statistician, and W. Allen Wallis (1912-1998), American economist and statistician. It is a non-parametric test and does not consider the hypotheses of comparison of the parameters, does not test the hypothesis of equality of averages or tests the equality of median. Kruskal-Wallis test is used to compare ordinal or continuous variables, and is indicated to assess the hypothesis that three or more samples have or not similar distribution (KRUSKAL et al., 1952).

The test is based on the hypothesis that the medians of the samples are equal. However, only through the test it is not possible to identify which of the samples differs from the other, and it is only possible to identify that there is a statistically significant difference between them. Therefore, to identify which of the samples is different, you need to perform a multiple comparison test, such as the Dunn Post-Hoc test (PONTES, 2000).

Dunn's post-hoc test is a multiple comparison statistical test used to compare the median of two or more independent samples after performing the Kruskal-Wallis test. It is based on the hypothesis that the median samples are similar.

For the Dunn test you need to notice:

- H0: The median are equal (among the subgroups analyzed)
- H1: The median are different

53
ISSN eletrônico 2177-2738
RA'EGA, Curitiba, PR, V.60, n.1, p. 45 – 69, 8/2024
http://dx.doi.org/10.5380/raega.v60i0.95709

p-value 0.05:

- If p-value <0.05, h0 is rejected (then, it is concluded that the median ones are different)
- If p-value> = 0.05, H0 is accepted (then, it is concluded that the median ones are equal)

III. RESULTS AND DISCUSSION

Rainfall analysis

The total annual rainfall, according to the climatological normal (CN 1991-2020) of the region, is 2459.75 mm and has shown a well-defined seasonality (Figure 3A). There was a dry period (June to August, shaded area) and a rainy (October to April) with higher and lowest rainfall observed in January (337.41 mm) and July (39.74 mm), respectively. In the years of the study, all of them have presented low total climatological rainfall, highlighting 2005, 2010 and 2015, which had negative anomalies of -226, -273 and -354 mm, respectively (Figures 3C, 3D and 3E). Despite of 2000 and 2020 had presented negative anomalies of rainfall, it happened in specific months and not for a long period.

In the first two decades of the 21st century, the Amazon region has undergone three major drought events in the years of 2005, 2010 and 2015 (SHE et al., 2024). The same authors also stated that these droughts varied not only in intensity, but also in the mechanisms that caused them. Among the three events, 2010 stood out for being the most severe while the 2005 was the one that had the least impact on the physiological and structural perspective of the Amazon rainforest. The 2015 drought was caused by the El Niño event, which was considered one of the three strongest that was observed within the period of climate records (SOUZA et al., 2022a and 2022b). However, in the years 2005 and 2010, the temperature in the Equatorial region of the Pacific Ocean had conditions of neutrality and the drought was caused by heating the North Atlantic waters (ZENG et al., 2008). According to the same authors, these droughts caused several impacts on transportation, fishing, agriculture, burning occurrences and the health of the local population.

It is noteworthy that both events, El Niño and the Atlantic heating, are responsible for modifying the general circulation of the atmosphere, especially in the circulation of Walker and Hardley cells and, generally, intensify dry air subsidence on the Amazon, inhibiting the deep convective clouds formation and, consequently, rainfall formation (ZENG et al., 2008). The authors also observed that during these events, there was a reduction in the transport of Atlantic moisture to the Amazon, which usually flows to the west, ascending in the Amazon and is deviated along the Andes to the south.

O ESPAÇO GEOGRÁFICO EM ANÁLISE
https://revistas.ufpr.br/raega
ISSN eletrônico 2177-2738
RA'EGA, Curitiba, PR, V.60, n.1, p. 45 – 69, 8/2024
http://dx.doi.org/10.5380/raega.v60i0.95709

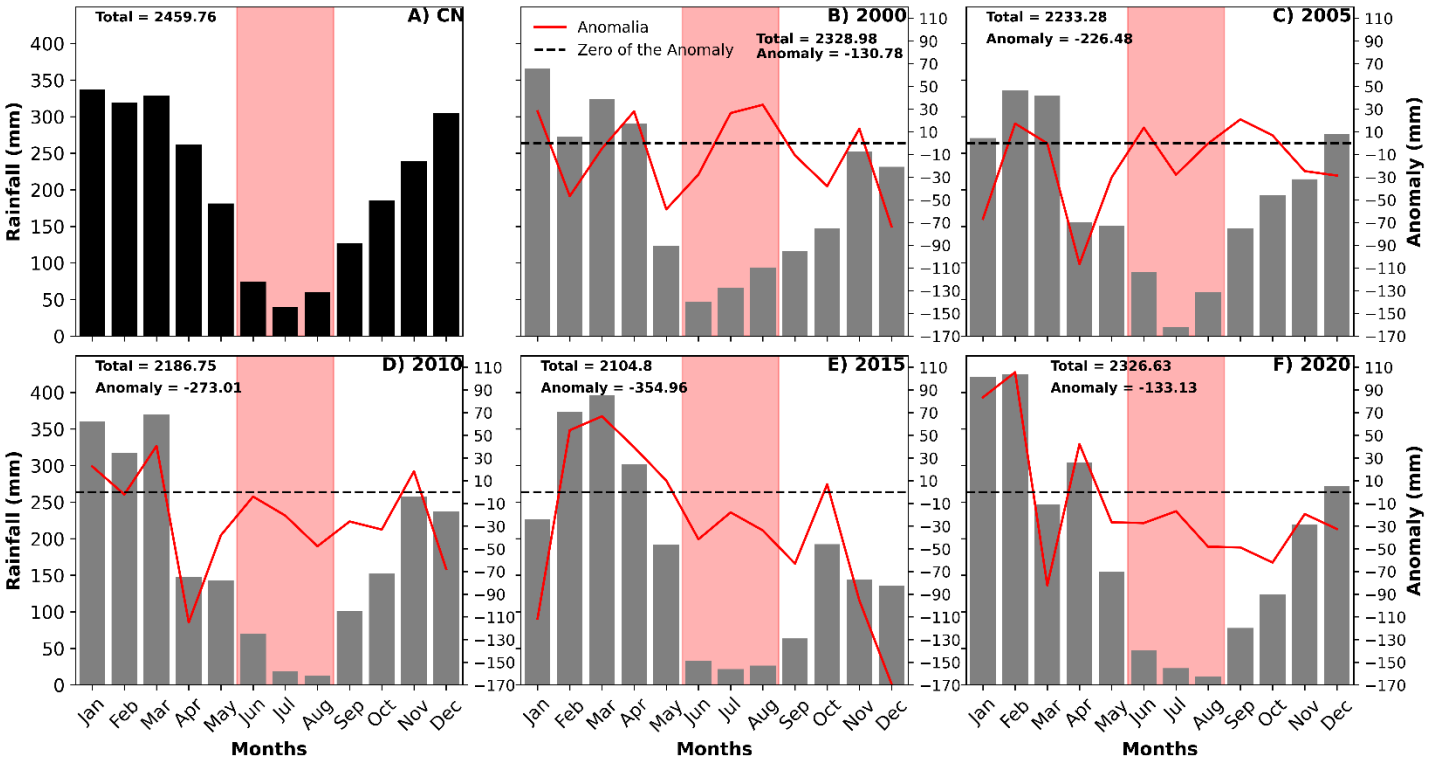

Figure 3 – Rainfall Climatological Normal (CN), monthly total rainfall and monthly rainfall anomaly for the years of 2000 (B), 2005 (C), 2010 (D), 2015 (E) and 2020 (F), for the municipality of Humaitá, Amazonas, Brazil. Shadowed area corresponds to the months of the dry period.

Soil Heat Flux (G)

The highest G values were found in the regions of Natural Field and Farm, with an average of approximately 48 W m^{-2} for both areas. In natural fields, the maximum average value was 63.81 W m^{-2} and the minimum average was 26.66 W m^{-2} while for soy farm was 61.30 W m^{-2} and 27.75 W m^{-2} for maximum and minimum averages, respectively. The areas of natural field and farm presented in the second quartile (Q2) the median of 45.5 W m^{-2} and 43.7 W m^{-2} respectively, and in the third quartile (Q3) was 52.6 W m^{-2} for both areas. The average values of G in the forest region were approximately 30 W m^{-2}, with maximum averages of 43.73 W m^{-2} and a minimum of 21.18 W m^{-2}. In Q2, the median was of 27.7 W m^{-2} and in Q3 was of 43.8 W m^{-2}. The Kuskal-Wallis test showed that the samples are not from the same distribution, 5.00e^{-02} and p-value <= 1, ****: p <= 1.00e^{-04}. Dunn's test showed the similarity between field and farm, with a corrected P-value of 5.139e^{-02}. The test showed no similarity between the areas when compared to forest, with corrected p-value being 0 (Figure 4a).

For all areas of the study, it is noted that, from 2005, there is an increase in G fluxes, highlighting the year 2010 when the magnitude values were close to the 65 W m^{-2} in the forest and close to 80 W m^{-2} in field and farm area. The increase of G in the farm region began with soybean plantation (in the study region) in the

ISSN eletrônico 2177-2738
RA'EGA, Curitiba, PR, V.60, n.1, p. 45 – 69, 8/2024
http://dx.doi.org/10.5380/raega.v60i0.95709

years 2003/2005, when, up to 2018, the increase jumped from around 500 hectares of soy to 2000 hectares in the crop of 2019/2020 (CORREIO et al., 2019). The lowest values in the forest, when compared to other regions of study, in addition to the dense forest cover, which causes the decrease in the magnitude of G (Figure 4A), is caused by the existence of a litter layer on the soil, which makes the contact of the soil with the atmosphere (CARNEIRO et al., 2013). Yet, according to the same authors, the litter is quite common in the region of tropical forest and is characterized as a large reservoir of organic matter that has influence and aid in regulating much of the functional processes that occur in an ecosystem. The litter in forest areas is basically composed of leaves, roots, fruits, seeds, shrubs, grasses, stems, and other native plants, as well as animal waste.

When compared to interannual values, the highest values of 2010 are probably linked to the drought occurred at the time, as previously shown in Figure 3. The 2010 drought was widespread, affecting 57.7% of the Amazon rainforest, particularly in the West, Southeast and North borders (SHE et al., 2024). Moreover, according to the authors, photosynthetic activity, green and leaf area of Amazonian forests were suppressed in 2010. This suppression possibly resulted in decreased of the biomass accumulation rate above ground, as observed by Tian et al. (2023) in a tropical rainforest in China and, consequently, can increase the amount of energy that reaches the surface more directly and, for this reason, a generalization of G was observed (Figure 4D).

Studies regarding heat flow modeling in the soil by remote sensing have presented good results when compared to flux data measured *in situ*. Research conducted in the Mediterranean, in which the authors estimated, by remote sensing, surface energy balance, found an average 7% error for soil flow estimates when compared to *in situ* data (AWADA et al., 2024). Van Der Tol (2012) compared and validated in Spain, in an area like to savannah, satellite estimation with surface data. The author states that, in his validation, he found precise results when estimated the flow of soil heat over the discovered soil. According to the author, a comparison between remote sensing methods applied to radiometry was viable for the recovery of satellite-based terrestrial heat fluxes.

ISSN eletrônico 2177-2738
RA'EGA, Curitiba, PR, V.60, n.1, p. 45 – 69, 8/2024
http://dx.doi.org/10.5380/raega.v60i0.95709

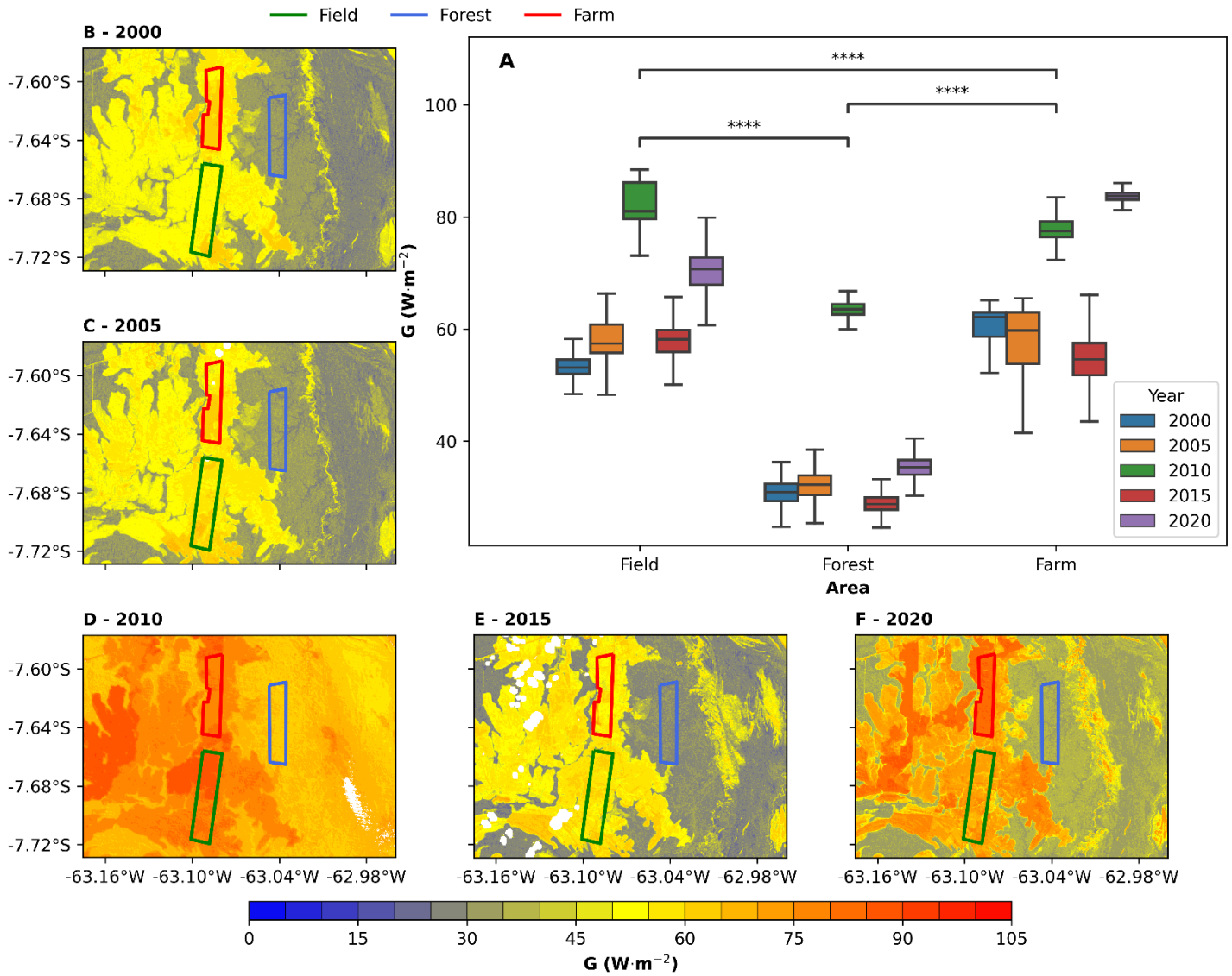

Figure 4 - Statistical Analysis of the Dunn's Test and Boxplot of the Soil Heat Flux (G) for Field, Farm and Forest (A) areas, and spatialization of G values for the years of 2000 (B), 2005 (C), 2010 (D), 2015 (E) and 2020 (F). **** correspond to the p-valor of the Kruskal-Wallis test.

Net Radiation (N_R)

The highest N_R values are concentrated in the forest region with average of 518.24 W m^{-2}, with maximum average of 559.3 W m^{-2} and minimum of 469.26 W m^{-2}, median Q2 of 506.6 W m^{-2} and Q3 of 530 W m^{-2}. The average N_R for field and farm area was very close, 493.6 m^{-2} and 485.27 W m^{-2}, respectively, and the medians Q2 was of 485.7 W m^{-2} and Q3 of 502.3 W m^{-2} for field area, and Q2 equal to 476.9 W m^{-2} and Q3 of 494 W m^{-2} for farm (Figure 5A). It was noted that in all areas the highest N_R values were concentrated in 2010 and 2015, except for the farm area, which obtained the highest value in 2020 and not in 2015. The lowest values occurred, for all sites, in 2005 and was observed in the agricultural area, with a magnitude of approximately 450 W m^{-2}.

ISSN eletrônico 2177-2738
RA'EGA, Curitiba, PR, V.60, n.1, p. 45 – 69, 8/2024
http://dx.doi.org/10.5380/raega.v60i0.95709

The Kuskal-Wallis test showed that the samples are not from the same distribution (****: p <0.05). Dunn's test showed the similarity between field and forest and pointed to p-value p < 0.05. The test showed no similarity between the areas when compared to forest, with corrected p-value being 0.

The areas where there is little vegetation and less water availability (fields and farm), when compared to forests, tend to have lower values of shortwave balance because they have greater superficial albedo, resulting in a low N_R (QUERINO et al., 2017). However, the opposite occurs when the vegetation is dense. In this case, regions such as forests have lower surface albedo and greater ability to absorb shortwave radiation and, consequently, higher values for N_R (SANTOS et al., 2011) (Figure 5A). The energy that is kept in the system is used in many physical, chemical, and biological processes, such as evapotranspiration, decomposition of organic matter among others (QUERINO et al., 2013; BIUDES et al., 2015)

Querino et al. (2016) have studied albedo and surface temperature, in the southwest region of the Amazon, and noticed that the low N_R values are a consequence of the highest albedo values and surface temperature in the forest. The authors observed that exposed soil areas, such as in field and farm, have presented smaller N_R and attributed to a larger amount of energy that is reflected to the space, thus less energy remains available to the biophysical and chemical processes of surface.

N_R is formed by the balance of short and longwave on a particular surface. Shortwave balance is controlled by incident and reflected solar radiation on a surface, as explained earlier. The longwave component is directly related to the surface temperature (in this case, Earth's surface) or environment, such as the atmosphere (QUERINO et al., 2020). The lowest surface temperature in the forest area contributes to increasing the balance of long waves and, thus, to increase N_R (FAUSTO et al., 2014). Hence, the high values of N_R, in a forest area, are direct combination of low superficial albedo values, greater amount of water, higher vegetation index and lower surface temperature (MARQUES et al., 2017).

The interannual variability of N_R may be attributed to specific climate conditions of each year. In the dry condition, especially when it occurs in the rainy season, causes suppression in cloud formation and higher incidence of solar radiation and, thus, tends to increase the balance of shortwaves (ZENG et al., 2008). Drought situations completely modify the amount of precipitation (Figure 3), as well as favors the increase of the surface and air temperature (SHE et al., 2024).

ISSN eletrônico 2177-2738
RA'EGA, Curitiba, PR, V.60, n.1, p. 45 – 69, 8/2024
http://dx.doi.org/10.5380/raega.v60i0.95709

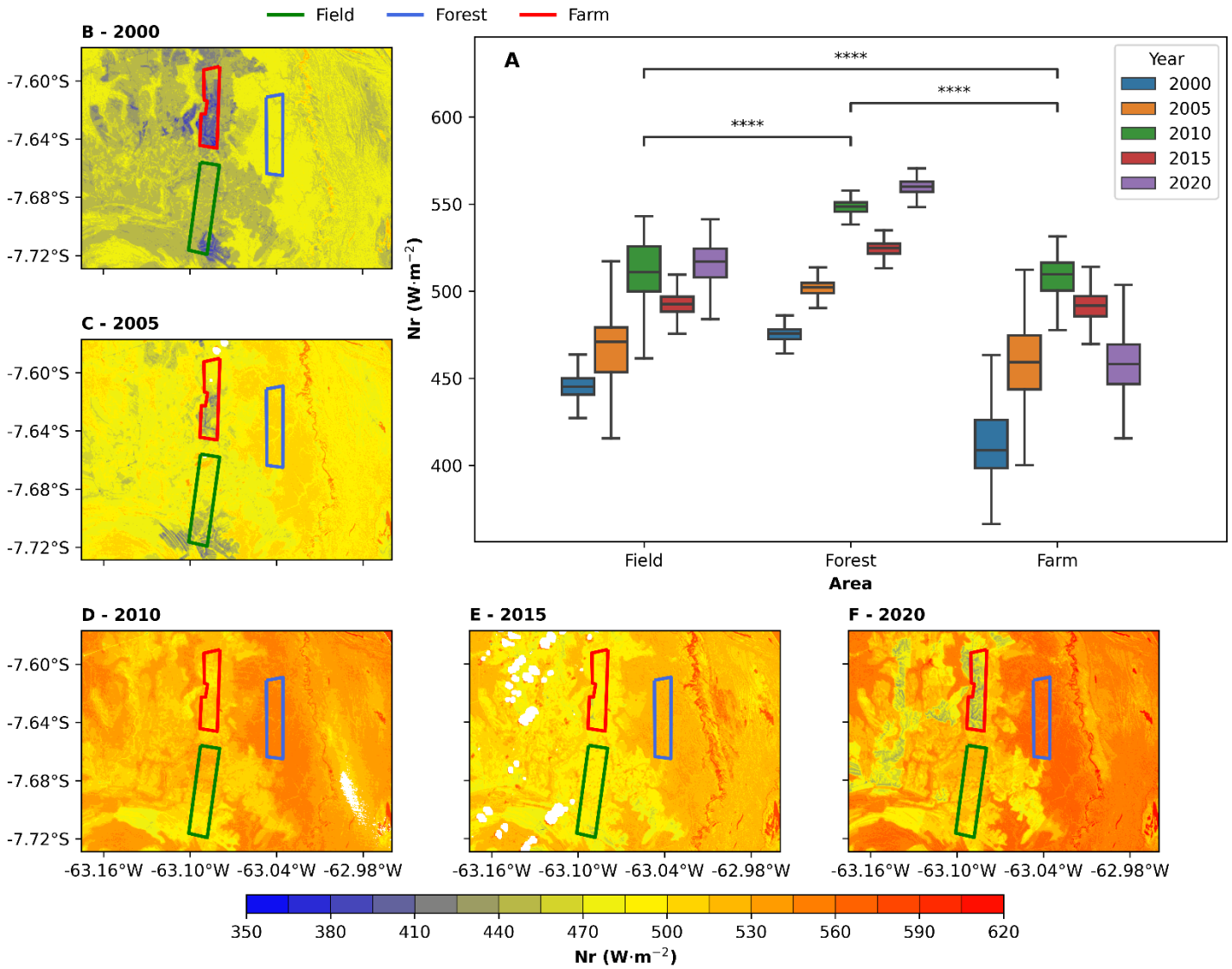

Figure 5 - Statistical Analysis of the Dunn's Test and Boxplot of the Net Radiation (N_R) for Field, Farm and Forest areas (A) and Spatialization of N_R values for the years of 2000 (B), 2005 (C), 2010 (D), 2015 (E) and 2020 (F). **** correspond to the p-valor of the Kruskal-Wallis test.

Sensible (H) *and* Latent (LE) Heat Fluxes

The highest average values of H were observed in regions that have lower vegetative coverage, i.e. in fields (333.17 W m^{-2}) and farm (279.06 W m^{-2}). In the fields, the median Q2 was of 287.2 W m^{-2} and Q3 was of 403 W m^{-2}, while for farm, the quartiles presented slightly smaller median, 201 W m^{-2} for Q2 and 376 W m^{-2} for Q3. It was observed that, in addition to the lowest average values, the forest also presented the smallest medians with Q2 of 63.5 W m^{-2} and Q3 of 170.6 W m^{-2}. *LE* flux was contrary to the H flux, which meant that it has presented the lowest average values for the regions with the smaller amount of vegetation, field and farm

ISSN eletrônico 2177-2738
RA'EGA, Curitiba, PR, V.60, n.1, p. 45 – 69, 8/2024
http://dx.doi.org/10.5380/raega.v60i0.95709

(Figure 6). For field and farm areas, the observed medians for Q2 were of 43.3 W m^{-2} and 154 W m^{-2} and for Q3 of 32.8 W m^{-2} and 237.6 W m^{-2}, respectively. On the other hand, for forest, the smallest averages were approximately 400 W m^{-2} and the maximums of 500 W m^{-2}.

As it occurs with all the other variables, the Kuskal-Wallis test has showed that *H* and *LE* samples are not from the same distribution, ****: p <= 0.05. Dunn's test showed the similarity between fields and farm, with a corrected p-value also less than 0.05. The test showed no similarity between the areas when compared to forest, with corrected p-value equal to 0 (Figures 6 and 7).

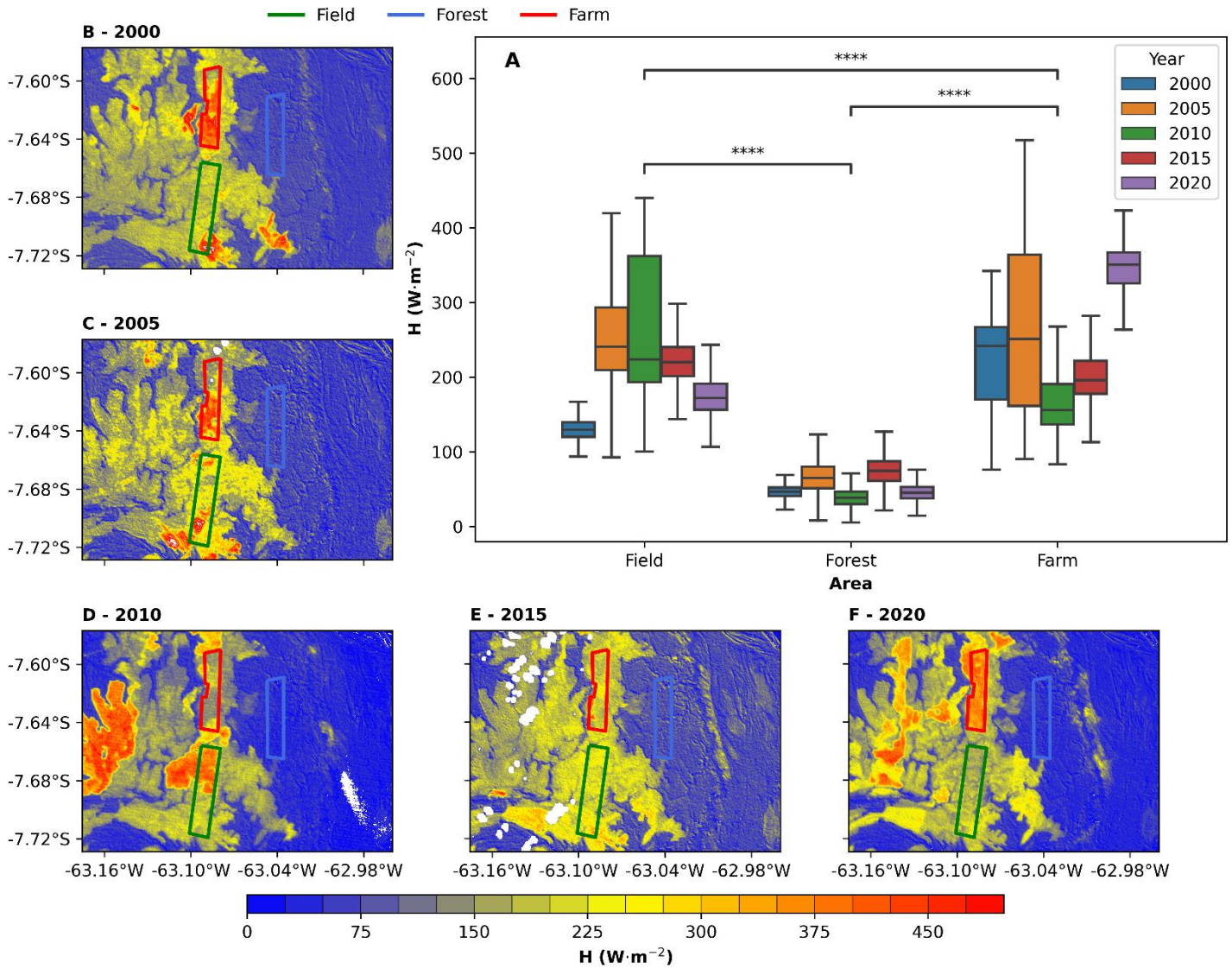

Figure 6 - Statistical Analysis of the Dunn's Test and Boxplot of Sensible Heat Flux (*H*) for field, Farm and Forest areas (A) and spatialization of *H* values for the years 2000 (B), 2005 (C), 2010 (D), 2015 (E) and 2020 (F). **** correspond to the p-valor of the Kruskal-Wallis test.

ISSN eletrônico 2177-2738
RA'EGA, Curitiba, PR, V.60, n.1, p. 45 – 69, 8/2024
http://dx.doi.org/10.5380/raega.v60i0.95709

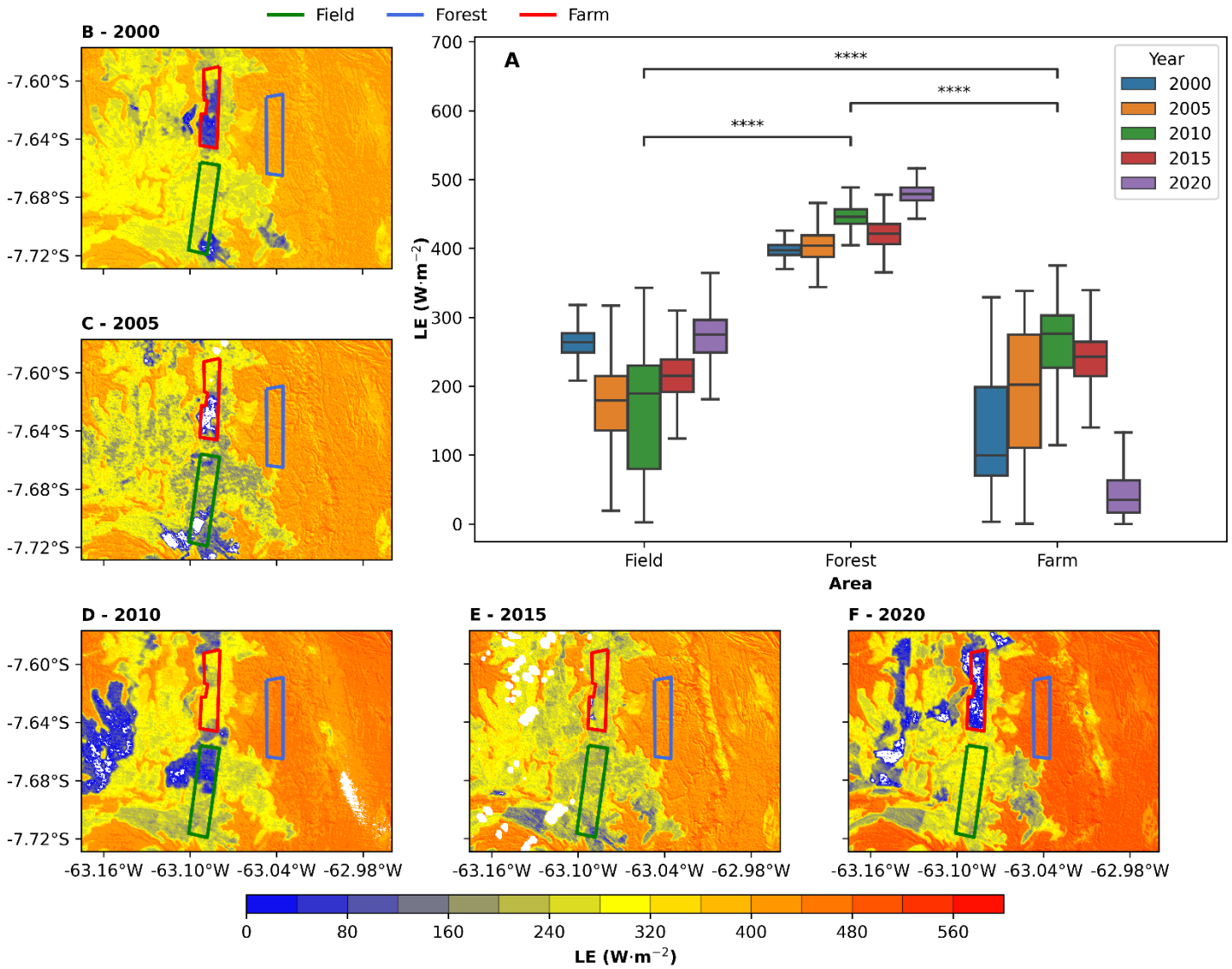

Figure 7 - Statistical Analysis of the Dunn's Test and Boxplot of Latent Heat Flux (*LE*) for Field, Farm and Forest areas (A) and spatialization of *LE* values for the years 2000 (B), 2005 (C), 2010 (D), 2015 (E) and 2020 (F). **** correspond to the p-valor of the Kruskal-Wallis test.

Study comparing estimates of sensitive and latent satellite heat fluxes with terrestrial measurements, in savannah vegetation in Australia, showed that the estimated values of *H* and *LE* presented differences according to the reported in the literature (BAZARRA et al., 2019). Also, according to authors, these results indicate that assimilation of the sequences of Copernicus product, such as those of ERA5-LAND, can help in partitioning of sensitive and latent heat fluxes, which allows to use them in the models for studies of these variables in areas that do not have surface data, such as the areas proposed in this article.

In the field and the farm, there is a tendency to less availability of water vapor, when compared to the forest that has extensive vegetative cover. Thus, the lowest *H* values are environmental responses to G and N_R, and amount of water available in each environment. Most of the energy absorbed in the forest is used in the

ISSN eletrônico 2177-2738
RA'EGA, Curitiba, PR, V.60, n.1, p. 45 – 69, 8/2024
http://dx.doi.org/10.5380/raega.v60i0.95709

diverse physical, chemical, and biological processes. Thus, most of the energy is used by plants in evapotranspiration processes that cause the decrease in *H* and, consequently, cools the vegetated surface and air near its proximities (BIUDES et al., 2015; ANGELINI et al., 2021). Studies on energy balance in deciduous forests in the United States pointed out that part of the water contained in the system is used in the forest growth processes and carbon assimilation and, consequently, are released in the evapotranspiratory process in the form of LE (ELIZABETH and ARAIN, 2023).

The forest area had the highest values for LE, which is due to the higher availability of water vapor on the surface, which does not occur in the fields and farm areas, which are locations with the most exposed soil and less availability of steam water. In any case, both sensitive and latent heat flow tends to follow the availability of N_R (VENÄLÄINEN et al., 1999). The authors observed that the highest H flows occurred near noon and *LE* reduced in the dry years. Probably, the decrease in *LE* is related to decreased moisture, even in the forest region, due to the reduction in precipitation (Figure 3), as observed by Ataide et al. (2020). The difference in energy partitioning among the environments studied here may be related to elements of environmental stress. Variables such as climate (periods of dried such as those presented in Figure 3) and the phenological cycle of all sites can have significant impacts on water use in each environment, reducing *LE* and increases *H* (SETT et al., 2023). The same authors also stated that different plant species, under similar geographical conditions, with different climatic conditions, presented different physiological responses, depending on each plant species that have unique characteristics and, consequently, impact the partitioning of sensitive heat flows and latent.

IV. CONCLUSIONS

The work sought to compare the energy balance components, estimated by SEBAL, in areas of forest, fields and soybean farm. The results showed similarity to the surface energy balance for field and farm because they had less dense vegetation, which allows greater soil exposure, and distinguished themselves from the forest areas. These similarities and differences between the areas were explained by the Dunn's test, which showed, through the adjusted p-value, a similarity between the energy balance components between the field and farm areas and, difference when compared to the forest areas.

In the interannual comparisons, the climate factor was evident. The years that had more intense rainfall deficit directly impacted the heat fluxes on the soil and N_R and, therefore, on the *H* and LE energy components.

ISSN eletrônico 2177-2738
RA'EGA, Curitiba, PR, V.60, n.1, p. 45 – 69, 8/2024
http://dx.doi.org/10.5380/raega.v60i0.95709

The impact of the change on land coverage was evidenced when there is a conversion of forest areas into areas of cultivation. However, the study shows that there is almost no impact on the energy balance if there is a replacement of natural fields in soybean cultivation areas.

V. REFERENCES

ALLEN, R.; IRMAK, A.; TREZZA, R.; HENDRICKX, J. M. H.; BASTIAANSSEN, W.; KJAERSGAARD, J. Satellite-based ET estimation in agriculture using SEBAL and METRIC. Hydrological Processes, v. 25, n. 26, 2011, p. 4011–4027. https://doi.org/10.1002/hyp.8408.

ANDRADE, M. B. T.; FERRANTE, L.; FEARNSIDE, P. M. Brazil's Highway BR-319 demonstrates a crucial lack of environmental governance in Amazonia. In Environmental Conservation. v. 48, n. 3, 2021 p. 161–164. Cambridge University Press. https://doi.org/10.1017/S0376892921000084.

ANGELINI, L. P.; BIUDES, M. S.; MACHADO, N. G.; GELI, H. M. E.; VOURLITIS, G. L.; RUHOFF, A.; NOGUEIRA, J. de S. Surface albedo and temperature models for surface energy balance fluxes and evapotranspiration using Sebal and Landsat 8 over Cerrado-Pantanal, Brazil. Sensors, 21 (21), 2021. https://doi.org/10.3390/s21217196.

ARYALEKSHMI, B. N.; BIRADAR, R. C.; CHANDRASEKAR, K.; MOHAMMED AHAMED, J. Analysis of various surface energy balance models for evapotranspiration estimation using satellite data. In Egyptian Journal of Remote Sensing and Space Science, v. 24, n. 3, 2021, p. 1119–1126. Elsevier B.V. https://doi.org/10.1016/j.ejrs.2021.11.007.

ATAIDE, W. L. S.; OLIVEIRA, F. S.; PINTO, C. A. Balanço de radiação, energia e fechamento do balanço em uma floresta prístina na Amazônia oriental. Revista Brasileira de Geografia Física, v. 13, 2020, p. 2603-2627. https://doi.org/10.26848/rbgf.v13.6.p2603-2627.

AWADA H., SIRCA, C.; MARRAS, S.; CASTELLINI, M.; SPANO D.; PIRASTRU M. Modelling soil moisture and daily actual evapotranspiration: Integrating remote sensing surface energy balance and 1D Richards equation. International Journal of Applied Earth Observation and Geoinformation, v. 128, 103744, 2024, p. 1-12. https://doi.org/10.1016/j.jag.2024.103744.

BARBER, C. P.; COCHRANE, M. A.; SOUZA, C. M.; LAURANCE, W. F. Roads, deforestation, and the mitigating effect of protected areas in the Amazon. Biological Conservation, v. 177, 2014 p.203–209. https://doi.org/10.1016/j.biocon.2014.07.004.

BARRAZA, V.; GRINGS, F.; FRANCO, M.; DOUNA, V.; ENTEKHABI, D.; RESTREPO-COUPE, N.; HUETE, A.; GASSMANN, M.; ROITBERG, E. Estimation of latent heat flux using satellite land surface temperature and a variational data assimilation scheme over a eucalypt forest savanna in Northern Australia. Agricultural and Forest Meteorology, v. 268, p. 341-353. ISSN 0168-1923. https://doi.org/10.1016/j.agrformet.2019.01.032.

BASTIAANSEEN, W. G. M.; MENENTI, M.; FEDDES, R. A.; HOLTSLAG, A. A. M. A Remote Sensing Surface Energy Balance Algorithm for Land (SEBAL) 1. Formulation. Journal of Hydrology, vol. 212-213, 1998, p. 198-212. https://doi.org/10.1016/S0022-1694(98)00253-4.

BASTIAANSSEN, W. G. M. SEBAL-based sensible and latent heat fluxes in the irrigated Gediz Basin, Turkey. Journal of Hydrology, vol. 229, n. 1-2, 2000, p. 87-100. https://doi.org/10.1016/S0022-1694(99)00202-4.

BASTIAANSSEN, W. G. M.; NOORDMAN, E. J. M.; PELGRUM, H.; DAVIDS, G.; THORESON, B. P.; ALLEN, R. G. SEBAL

ISSN eletrônico 2177-2738
RA'EGA, Curitiba, PR, V.60, n.1, p. 45 – 69, 8/2024
http://dx.doi.org/10.5380/raega.v60i0.95709

Model with Remotely Sensed Data to Improve Water-Resources Management under Actual Field Conditions. Journal of Irrigation and Drainage Engineering, v. 131, n. 1, 2005, p. 85–93. https://doi.org/10.1061/(ASCE)0733-9437(2005)131:1(85).

BECK, H. E.; VAN DIJK, A. I. J. M.; LEVIZZANI, V.; SCHELLEKENS, J.; MIRALLES, D. G.; MARTENS, B.; de ROO, A. MSWEP: 3-hourly 0.25° global gridded precipitation (1979-2015) by merging gauge, satellite, and reanalysis data. Hydrology and Earth System Sciences, v. 21, n. 1, 2017, p. 589–615. https://doi.org/10.5194/hess-21-589-2017.

BHATTARAI, N.; LIU, T. LandMOD ET mapper: A new matlab-based graphical user interface (GUI) for automated implementation of SEBAL and METRIC models in thermal imagery. Environmental Modelling and Software, vol. 118, 2019p. 76–82. https://doi.org/10.1016/j.envsoft.2019.04.007.

BIUDES, M. S.; VOURLITIS, G. L.; MACHADO, N. G.; de ARRUDA, P. H. Z.; NEVES, G. A. R.; de ALMEIDA LOBO, F.; NEALE, C. M. U.; de SOUZA NOGUEIRA, J. Patterns of energy exchange for tropical ecosystems across a climate gradient in Mato Grosso, Brazil. Agricultural and Forest Meteorology, vol. 202, 2015, p. 112–124. https://doi.org/10.1016/j.agrformet.2014.12.008.

CAMPOS, M. B. de L. M. B.; DANELICHEN, V. H. M. Sensoriamento Remoto e Estudos de Clima Urbano. Ensaios e Ciência Biológicas Agrárias e da Saúde, v. 25, n. 2, 2021, p. 195–199. https://doi.org/10.17921/1415-6938.2021v25n2p195-199.

CARNEIRO, R. G.; MOURA, M. A. L.; LYRA, R. F. DA F.; ANDRADE, A. M. D. DE; SANTOS, A. B. DOS; MAIA, R. G. X. Fluxo de calor do solo e saldo de radiação dentro de uma área de Mata Atlântica em comparação com uma área de cana-de-açúcar. Revista Brasileira de Geografia Física, v. 6, n. 3, 2013, p. 555-565. https://doi.org/10.26848/rbgf.v6.3.p555-565.

CARNEIRO, R. G.; BORGES, C. K.; SANTOS, C. A.; de OLIVEIRA, G.; STACHLEWSKA, I. S.; FISCH, G.; dos SANTOS, C. A. C. Energy balance closure and evapotranspiration hysteresis in central Amazon under contrasting conditions during the GoAmazon project in 2014 and 2015. Journal of South American Earth Sciences, v. 132, 2023, p. 104686. ISSN 0895-9811. https://doi.org/10.1016/j.jsames.2023.104686.

CHANG, Y.; DING, Y.; ZHAO, Q.; ZHANG, S. Remote estimation of terrestrial evapotranspiration by Landsat 5 TM and the SEBAL model in cold and high-altitude regions: a case study of the upper reach of the Shule River Basin, China. Hydrological Processes, v. 31, n. 3, 2017, p. 514-524. https://doi.org/10.1002/hyp.10854.

CORRÊA, P. B.; CÂNDIDO, L. A.; de SOUZA, R. A. F.; ANDREOLI, R. V.; KAYANO, M. T. Heat islands in Manaus City: Study with remote sensing data, modeling and meteorological data. Revista Brasileira de Meteorologia, vol. 31, n. 2, 2016, p. 167–176. https://doi.org/10.1590/0102-778631220150012.

COSTA JÚNIOR, V. G.; SANTOS, C. A. C. dos; SILVA, T. L. do V. Balanço de energia à superfície em áreas heterogêneas através de algoritmos de sensoriamento remoto. Revista Brasileira de Geografia Física, v. 10, n. 2, 2017, p. 454-467. https://doi.org/10.5935/1984-2295.20170028.

DOMINGUES, M. S.; BERMANN, C. O arco de desflorestamento na Amazônia: da pecuária à soja. Ambiente & Sociedade, v. 15, n. 2, 2012, p. 1–22. https://doi.org/10.1590/S1414-753X2012000200002.

ELIZABETH, A. R.; ARAIN, M. A. Impacts of heat and drought on the dynamics of water fluxes in a temperate deciduous forest from 2012 to 2020. Agricultural and Forest Meteorology, v. 344, 2024, p. 109791. ISSN 0168-1923. https://doi.org/10.1016/j.agrformet.2023.109791.

FAUSTO, M. A.; MACHADO, N. G.; NOGUEIRA, J. S.; BIUDES, M. S. Net radiation estimated by remote sensing in

ISSN eletrônico 2177-2738
RA'EGA, Curitiba, PR, V.60, n.1, p. 45 – 69, 8/2024
http://dx.doi.org/10.5380/raega.v60i0.95709

Cerrado areas in the Upper Paraguay River Basin. Journal of Applied Remote Sensing, vol. 8, 2014, p. 083541.

FEARNSIDE, P. Deforestation of the Brazilian Amazon. In Oxford Research Encyclopedia of Environmental Science. Oxford University Press, 2017, p. 1-49. https://doi.org/10.1093/acrefore/9780199389414.013.102.

FIEDLER, F.; PANOFSKY, H. A. The geostrophic drag coefficient and the 'effective' roughness length. Quarterly Journal of the Royal Meteorological Society, v. 98, n. 415, p. 213–220, 1972. https://doi.org/10.1002/qj.49709841519.

GÓMEZ, M.; OLIOSO, A.; SOBRINO, J. A.; JACOB, F. Retrieval of evapotranspiration over the Alpilles/ReSeDA experimental site using airborne POLDER sensor and a thermal camera. Remote Sensing of Environment, v. 96, n. 3–4, 2005, p. 399–408. https://doi.org/10.1016/j.rse.2005.03.006.

GONÇALVES, I. Z.; RUHOFF, A.; LAIPELT, L.; BISPO R. C.; HERNANDEZ, F. B. T.; NEALE, C. M. U.; TEIXEIRA, A. H. C.; MARIN, F. R. Remote sensing-based evapotranspiration modeling using geeSEBAL for sugarcane irrigation management in Brazil. Agricultural Water Management, v. 274, 2022, p. 1-12. ISSN 0378-3774, https://doi.org/10.1016/j.agwat.2022.107965.

Instituto Brasileiro de Geografia e Estatística (IBGE). 2017. Disponível em: https://www.ibge.gov.br. Acesso em: 3 mai. 2022.

Instituto de Desenvolvimento Agropecuário e Florestal Sustentável do Estado do Amazonas (IDAM). 2018. Disponível em: https://www.idam.gov.br. Acesso em: 10 mai. 2022.

Instituto de Desenvolvimento Agropecuário e Florestal Sustentável do Estado do Amazonas (IDAM). 2020. Disponível em: https://www.idam.gov.br. Acesso em: 22 de set. 2023.

JAAFAR, H. H.; AHMAD, F. A. Time series trends of Landsat-based ET using automated calibration in METRIC and SEBAL: The Bekaa Valley, Lebanon. Remote Sensing of Environment, v. 238, 2021, p. 111034. https://doi.org/10.1016/j.rse.2018.12.033.

KREBS-KANZOW, U.; GIERZ, P.; RODEHACKE, C. B.; XU, S.; YANG, H.; LOHMANN, G. The diurnal Energy Balance Model (dEBM): A convenient surface mass balance solution for ice sheets in Earth system modeling. Cryosphere, v. 15, n. 5, 2021, p. 2295–2313. https://doi.org/10.5194/tc-15-2295-2021.

KRUSKAL, W. H.; WALLIS, W. A. Use of Ranks in One-Criterion Variance Analysis. Journal of the American Statistical Association, vol. 47, n. 260, 1952, p. 583-621. dx.doi.org/10.1080/01621459.1952.10483441.

LAIPELT, L.; KAYSER, R. H. B.; FLEISCHMANN, A. S.; RUHOFF, A.; BASTIAANSSEN, W.; ERICKSON, T. A.; MELTON, F. Long-term monitoring of evapotranspiration using the SEBAL algorithm and Google Earth Engine cloud computing. ISPRS Journal of Photogrammetry and Remote Sensing, v. 178, 2021, p. 81–96. https://doi.org/10.1016/j.isprsjprs.2021.05.018.

LI, G.; JING, Y.; WU, Y.; ZHANG, F. Improvement of two evapotranspiration estimation models using a linear spectral mixture model over a small agricultural watershed. Water (Switzerland), vol. 10, n. 4, 2018, p. 1-17. https://doi.org/10.3390/w10040474.

LI, Y.; KUSTAS, W. P.; HUANG, C.; NIETO, H.; HAGHIGHI, E.; ANDERSON, M. C.; DOMINGO, F.; GARCIA, M.; SCOTT, R. L. Evaluating Soil Resistance Formulations in Thermal-Based Two-Source Energy Balance (TSEB) Model: Implications for Heterogeneous Semiarid and Arid Regions. Water Resources Research, v. 55, n. 2, 2019, p. 1059-1078. https://doi.org/10.1029/2018WR022981.

LIMA, M. do S. B. de. Políticas públicas e territórios: uma discussão sobre os determinantes da soja no sul do

ISSN eletrônico 2177-2738
RA'EGA, Curitiba, PR, V.60, n.1, p. 45 – 69, 8/2024
http://dx.doi.org/10.5380/raega.v60i0.95709

Amazonas. 390f. Tese. (Doutorado em Geografia) – Universidade Federal Rural do Rio de Janeiro, Rio de Janeiro, 2008.

MACHADO, C. C.; SILVA, B. B. da; ALBUQUERQUE, M. de B.; Domiciano Galvíncio, J. Estimativa do balanço de energia utilizando imagens Tm-Landsat 5 e o algoritmo Sebal no litoral Sul de Pernambuco. Revista Brasileira de Meteorologia, vol. 29, n. 1, 2014 p. 55 - 67.

MARQUES, H. O. Estimativa do saldo de radiação de uma floresta de transição Amazônia-Cerrado por Sensoriamento Remoto. 53 f. Dissertação (Mestrado em Física Ambiental) - Universidade Federal de Mato Grosso, Cuiabá, 2015.

MARQUES, H. O.; BIUDES, M. S.; PAVÃO, V. M.; MACHADO, N. G.; QUERINO, C. A. S.; DANELICHEN, V. H. de M. Estimated net radiation in an Amazon–Cerrado transition forest by Landsat 5 TM. Journal of Applied Remote Sensing, v. 11, n. 04, 2017, p. 1046020-1 - 046020-12. https://doi.org/10.1117/1.jrs.11.046020.

MARTINS, P. A. da S. Normais Climatológicas, Balanço Hídrico e Classificação Climática para a Mesorregião Sul do Amazonas. 87 f. Dissertação (Mestrado em Ciências Ambientais) – Universidade Federal do Amazonas, Humaitá, 2019.

MARTINS, P. A. da S.; QUERINO, C. A. dos S.; QUERINO, J. K. A. da S.; MOURA, M. A. L.; NUNES, D. D.; MACHADO, N. G.; BIUDES, M. S. Updating of the Köppen and Thornthwaite and Mather (1955) climate classification system for the Southern Amazonas. Revista do Departamento de Geografia da USP, vol. 43, 2023, p. 1-13 e191137. https://doi.org/10.11606/eISSN.2236-2878.rdg.2023.191137.

MATSUNAGA, W. K.; RODRIGUES, H. J. B.; RODRIGUES, P. G. Microbiological attributes of the soil, associated to microfauna activities of soil in the Amazonia Forest. Anuário do Instituto de Geociências, v. 41, n. 3, p. 630–638. https://doi.org/10.11137/20183630638.

MIRANDA, E. de; CARVALHO, C. A. de; ROBERTO, P.; MARTINHO, R.; OSHIRO, O. T. Contribuições do geoprocessamento à compreensão do mundo rural e do desmatamento no bioma Amazônia. Colóquio - Revista do Desenvolvimento Regional-Faccat-Taquara/RS, vol. 17, n. 1, 2020, p. 16 - 34.

MOURA, A. R. de M.; QUERINO, C. A. S.; QUERINO, J. K. A. da S.; PEDREIRA JUNIOR, A. L.; SANTOS, L. O. F. dos; MACHADO, N. G.; BIUDES, M. S. Impact of a dam construction on the surface biophysical parameters in Amazonia. Remote Sensing Applications: Society and Environment, v. 15, 2019, p. 1 - 8. https://doi.org/10.1016/j.rsase.2019.100243.

MULLAN, K.; CAVIGLIA-HARRIS, J. L.; SILLS, E. O. Sustainability of agricultural production following deforestation in the tropics: Evidence on the value of newly-deforested, long-deforested and forested land in the Brazilian Amazon. Land Use Policy, v. 108, 2021, p. 1 - 13. https://doi.org/10.1016/j.landusepol.2021.105660.

NINA, M. M.; SANTOS, C. P. dos; ROCHA, S. F. da; CAVALCANTE, F. S. A.; LIMA, R. A. Potencialidade de Manihot esculenta Crantz (Euphorbiaceae) na Floresta Amazônica, Brasil. Diversitas Journal, v. 6, n. 2, 2021, p. 2247–2260. https://doi.org/10.17648/diversitas-journal-v6i2-1253.

O'BRIEN, P. L.; DAIGH, A. L. M. Tillage practices alter the surface energy balance – A review. In Soil and Tillage Research, v. 195, 2019, p. 1 - 7. Elsevier B.V. 2019. https://doi.org/10.1016/j.still.2019.104354.

PAVÃO, V. M.; QUERINO, C. A. S.; BENEDITTI, C. A.; PAVÃO, L. L.; QUERINO, J. K. A. da S.; MACHADO, N. G.; BIUDES, M. S. Variação espacial e temporal do saldo de radiação superficial em uma área do Sul do Amazonas. Revista Ra'e Ga –Curitiba, v. 37, 2016, p. 333-352.

ISSN eletrônico 2177-2738
RA'EGA, Curitiba, PR, V.60, n.1, p. 45 – 69, 8/2024
http://dx.doi.org/10.5380/raega.v60i0.95709

PEDREIRA JUNIOR, A. L.; QUERINO, C. A. S.; QUERINO, J. K. A. da S.; SANTOS, L. O. F. dos; MOURA, A. R. de M.; MACHADO, N. G.; BIUDES, M. S. Variabilidade horária e intensidade sazonal da precipitação no município de Humaitá–AM. Revista Brasileira de Climatologia, v. 22, 2018, p. 463 - 475. https://doi.org/10.5380/abclima.v22i0.58089.

PONTES, A. C. F. Obtenção dos níveis de significância para os testes de Kruskal-Wallis, Friedman e comparações múltiplas não-paramétricas. Dissertação (Mestrado em Estatística e Experimentação Agronômica) Biblioteca Digital (USP), 2000. https://doi.org/10.11606/D.11.2000.tde-15032002-093020.

QUERINO, C. A. S.; BENEDITTI, C. A.; MACHADO, N. G.; da SILVA, M. J. G.; QUERINO, J. K. A. da S.; NETO, L. A. dos S.; BIUDES, M. S. Spatiotemporal NDVI, LAI, albedo, and surface temperature dynamics in the southwest of the Brazilian Amazon forest. J. Appl. Remote Sens, v. 10, n.2, 2016, p. 026007. https://doi.org/10.1117/1.JRS.10.026007.

QUERINO, C. A. S.; BIUDES, M. S.; MACHADO, N. G.; QUERINO, J. K. A. S; MOURA, M. A. L.; ALVES, P. V. Modelling parametrization to estimate atmospheric long wave radiation in the Northern Mato Grosso, Brazil. Ciência e Natura, v. 42, 2020, p. e105.

QUERINO, C. A. S; BIUDES, M. S.; MACHADO, N. G.; QUERINO, J. K. A. S; SANTOS NETO, L. A.; SILVA, M. J. G. da, ARRUDA, P.; NOGUEIRA, J. S. Balanço de ondas curtas sobre floresta sazonalmente alagável do Pantanal Mato-Grossense. Revista Brasileira de Climatologia, vol. 20, 2017, p. 252-266.

QUERINO, C. A. S.; MOURA, M. A. L.; LYRA, R. F. F.; MARIANO, G. L. Avaliação e comparação de radiação solar global e albedo com ângulo zênital na região amazônica. Revista Brasileira de Meteorologia, v. 21, n. Especial, 2006, p. 42-49.

QUERINO, C. A. S.; MOURA, M. A. L.; QUERINO, J. K. A. da S. Impacto do desmatamento de uma área de mangue no albedo superficial. Revista Brasileira de Meteorologia, v. 28, 2013, p. 401-408.

REIS, F. da S.; ROCHA, K. da S. Áreas protegidas e o desmatamento no Sudoeste Amazônico: Método remoto de avaliação / Protected areas and deforestation in the southwest amazon: remote assessment method. Brazilian Journal of Development, v. 7, n. 12, 2022, p.121850–121865. https://doi.org/10.34117/bjdv7n12-785.

REIS, M. dos; GRAÇA, P. M. L. de A.; YANAI, A. M.; RAMOS, C. J. P.; FEARNSIDE, P. M. Forest fires and deforestation in the central Amazon: Effects of landscape and climate on spatial and temporal dynamics. Journal of Environmental Management, v. 288, 2021, p. 1 - 12. https://doi.org/10.1016/j.jenvman.2021.112310

ROCHA, N. S. da; KÄFER, P. S.; SKOKOVIC, D.; VEECK, G.; DIAZ, L. R.; KAISER, E. A.; CARVALHO, C. M.; CRUZ, R. C.; SOBRINO, J. A.; ROBERTI, D. R.; ROLIM, S. B. A. The influence of land surface temperature in evapotranspiration estimated by the s-sebi model. Atmosphere, v. 11 n. 10, 2020, p. 1 - 18. https://doi.org/10.3390/atmos11101059.

ROERINK, G. J.; SU, Z.; MENENTI, M. S-SEBI: A Simple Remote Sensing Algorithm to Estimate the Surface Energy Balance. Physics and Chemistry of the Earth, Part B, v. 25, n. 2, 2000, p. 147 - 157. https://doi.org/10.1016/S1464-1909(99)00128-8.

ROTHMUNDO, L. D; ALMEIDA JÚNIOR, E. S; LIMA, L. P. de A.; MASSAD, H. A. B.; PALÁCIOS, R. da S.; BIUDES, M. S; MACHADO, N. G, NOGUEIRA, J. S. Impacto da alteração da cobertura do solo nos parâmetros biofísicos no Sul da Floresta Amazônica por sensoriamento remoto. Revista Brasileira de Climatologia. vol. 25, n. jul/dez, 2019, p. 122 - 137. https://doi.org/10.5380/abclima.v25i0.62677.

ISSN eletrônico 2177-2738
RA'EGA, Curitiba, PR, V.60, n.1, p. 45 – 69, 8/2024
http://dx.doi.org/10.5380/raega.v60i0.95709

RUHOFF, A.; PAZ, A.; COLLISCHONN, W.; ARAGÃO, L.; ROCHA, H. S.; MALHI, Y. A MODIS Based Energy Balance to Estimate Evapotranspiration for Clear-Sky Days. In Brazilian Tropical Savannas, Remote Sensing, vol. 4, n. 3, 2012 p. 703-725. https://doi.org/10.3390/rs4030703.

SANTOS, C. A. dos; NASCIMENTO, R. L. do; RAO, T. V. R. Net radiation estimation under pasture and forest in Rondônia, Brazil, with TM Landsat 5 images. Atmósfera, v. 24, n. 4, 2011, p. 435-446.

SENAY, G. B.; BOHMS, S.; SINGH, R. K.; GOWDA, P. H.; VELPURI, N. M.; ALEMU, H.; VERDIN, J. P. Operational Evapotranspiration Mapping Using Remote Sensing and Weather Datasets: A New Parameterization for the SSEB Approach. Journal of the American Water Resources Association, v. 49, n. 3, 2013, p. 577–591. https://doi.org/10.1111/jawr.12057.

SETT, T.; NANDY, S.; PATEL, N. R.; PADALIA, H.; SRINET, R.; WATHAM, T. Spatio-temporal dynamics of water use efficiency over forest ecosystems using time series satellite data and carbon flux measurements. Forest Ecology and Management, v.548, 2023, p. 1 - 12. ISSN 0378-1127. https://doi.org/10.1016/j.foreco.2023.121385.

SHE, X.; LI, Y.; JIAO, W.; SUN, Y.; NI, X.; ZUO, Z.; KNYAZIKHIN, Y.; MYNENI, R. B. Varied responses of Amazon forests to the 2005, 2010, and 2015/2016 droughts inferred from multi-source satellite data. Agricultural and Forest Meteorology, v. 353, 2024, p. 1 - 10. ISSN 0168-1923. https://doi.org/10.1016/j.agrformet.2024.110051.

SILVA, C. A.; SANTILLI, G.; EYJI SANO, E.; RODRIGUES, S. W. P. Análise Qualitativa do Desmatamento na Floresta Amazônica a partir de Sensores SAR, Óptico e Termal (Qualitative Analysis of Deforestation in the Amazonian Rainforest from SAR, Optical and Thermal Sensors). Anuário do Instituto de Geociências (UFRJ), v. 42, n. 4, 2019, p. 18-29. https://doi.org/10.11137/2019_4_1_18_29.

SILVA, C. de O. F. da; MAGNONI, P. H. J.; MANZIONE, R. L. Sensoriamento remoto orbital para modelagem da evapotranspiração: síntese teórica e aplicações em computação na nuvem. Revista Brasileira de Engenharia de Biossistemas, v. 15, n. 3, 2021, p. 425–468. https://doi.org/10.18011/bioeng2021v15n3p425-468.

SILVA, V. V. da; ARAÚJO, J. N.; LIMA, L. A. P. O Agronegócio e as transformações na fronteira no Sul do Amazonas. In. Anais do XIV ENANPEGE. Campina Grande: Realize Editora, 2021.

SILVA, V. V. da; SILVA, R. G. da C.; LIMA, L. A. P. A estruturação da fronteira agrícola no Sul do estado do Amazonas. Geographia Opportuno Tempore, v.5, n. 1, 2019, p. 67–82. https://doi.org/10.5433/got.2019.v5.37193.

SINGH, R. K.; SENAY, G. B. Comparison of four different energy balance models for estimating EvapoTranspiration in the Midwestern United States. Water (Switzerland), v. 8, n. 1, 2016, p. 1 - 19. https://doi.org/10.3390/w8010009.

SONG, L.; LIU, S.; KUSTAS, W. P.; ZHOU, J.; XU, Z.; XIA, T.; LI, M. Application of remote sensing-based two-source energy balance model for mapping field surface fluxes with composite and component surface temperatures. Agricultural and Forest Meteorology, v. 230–231, 2016, p. 8–19. https://doi.org/10.1016/j.agrformet.2016.01.005.

SOUSA, A. C. de. Análise de Tendências e Fatores determinantes da intensificação de sistemas convectivos de mesoescala e linhas de instabilidade na costa Norte-Nordeste da América do Sul. 160 f. Tese (Doutorado em Clima e Ambiente) – Instituto Nacional de Pesquisas da Amazônia, Manaus, 2020.

SOUZA, S. A. S., QUERINO, C. A. S.; QUERINO, J. K. A. S.; MARTINS, P. A. S.; VAZ, M. A. B. Variabilidade da precipitação na mesorregião sul do Amazonas em decorrência de eventos de El Niño. Revista Ra'eGa - O Espaço Geográfico em Análise, v. 54, 2022, p. 23-36. http://dx.doi.org/10.5380/raega.v54i0.73972.

ISSN eletrônico 2177-2738
RA'EGA, Curitiba, PR, V.60, n.1, p. 45 – 69, 8/2024
http://dx.doi.org/10.5380/raega.v60i0.95709

SOUZA, S. A. S.; QUERINO, C. A. S; FERREIRA, N. C.; MOURA, M. A. L.; MARCELO, S. B.; MACHADO, N. G.; VOGT, R. H. M.; QUERINO, J. K. A. S.; ROHLEDER, L. A. S. Spatiotemporal variability of precipitation and surface temperature in the southern mesoregion of Amazonas, Brazil, during the occurrence of ENSO. Ciência e Natura, vol. 44, 2022, p. 1 - 20. http://dx.doi.org/10.5902/2179460x65690.

SU, Z. The Surface Energy Balance System (SEBS) for estimation of turbulent heat fluxes. Hydrology and Earth System Sciences, vol. 6, n. 1, 2002, p. 85 - 100. https://doi.org/10.5194/hess-6-85-2002.

TANG, R.; LI, Z. L.; CHEN, K. S.; JIA, Y.; LI, C.; SUN, X. Spatial-scale effect on the SEBAL model for evapotranspiration estimation using remote sensing data. Agricultural and Forest Meteorology, vol. 174–175, 2013, p. 28–42. https://doi.org/10.1016/j.agrformet.2013.01.008

TEIXEIRA, A. H. de C.; BASTIAANSSEN, W. G. M.; AHMAD, M. D.; BOS, M. G. Reviewing SEBAL input parameters for assessing evapotranspiration and water productivity for the Low-Middle São Francisco River basin, Brazil. Part A: Calibration and validation. Agricultural and Forest Meteorology, v. 149, n. 3–4, 2009, p. 462–476. https://doi.org/10.1016/j.agrformet.2008.09.016.

TIAN L.; TONG Y.; CHENG Y.; LI M; LETCHER S. G.; ZANG R.; DING Y. Drought diminishes aboveground biomass accumulation rate during secondary succession in a tropical forest on Hainan Island, China. Forest Ecology and Management, v. 544, 2023, p. 1 - 10. ISSN 0378-1127. https://doi.org/10.1016/j.foreco.2023.121222.

VAN DER TOL, C. Validation of remote sensing of bare soil ground heat flux. Remote Sensing of Environment, v. 121, 2012, p. 275-286. ISSN 0034-4257, 2012. https://doi.org/10.1016/j.rse.2012.02.009.

VARGHA, A.; DELANEY, H. D. The Kruskal-Wallis Test and Stochastic Homogeneity. Journal of Educational and Behavioral Statistics, vol. 23, n. 2, 1998, p. 170 - 192.

VELOSO, G. A. Análise espaço temporal dos componentes do balanço de radiação, energia e evapotranspiração, usando técnicas de sensoriamento remoto em áreas irrigadas do Projeto Jaíba/MG. 136f. Dissertação (Mestrado em Geografia) – Universidade Federal de Uberlândia, Uberlândia, 2014.

VELOSO, T.; SANTOS, D.; FONTANA, D. C.; CÁSSIA, R.; ALVES, M. Avaliação de fluxos de calor e evapotranspiração pelo modelo SEBAL com uso de dados do sensor ASTER (Evaluation of heat fluxes and evapotranspiration using SEBAL model with data from ASTER sensor). Pesq. agropec. bras. Brasília, vol. 45, n. 5, 2010, p. 488-496.

VENÄLÄINEN, A.; FRECH, M.; HEIKINHEIMO, M.; GRELLE, A. Comparison of latent and sensible heat fluxes over boreal lakes with concurrent fluxes over a forest: implications for regional averaging. Agricultural and Forest Meteorology, vol. 98–99, 1999, p. 535-546. ISSN 0168-1923. https://doi.org/10.1016/S0168-1923(99)00100-8.

VILA NOVA, R. A. Técnicas do sensoriamento remoto aplicadas a estudos ambientais. 78 f. Dissertação (Mestrado em Ciências Geodésicas e Tecnologias da Geoinformação) - Universidade Federal de Pernambuco - Centro de Tecnologia e Geociências, Recife, 2021.

WAGLE, P.; BHATTARAI, N.; GOWDA, P.H.; KAKANI, V.G. Performance of five surface energy balance models for estimating daily evapotranspiration in high biomass sorghum. ISPRS J. Photogramm. Remote Sens, vol. 128, 2017, p. 192–203. https://doi.org/https://doi.org/10.1016/j.isprsjprs.2017.03.022.

WEST, T. A. P.; FEARNSIDE, P. M. Brazil's conservation reform and the reduction of deforestation in Amazonia. Land Use Policy, vol.100, 2021, p. 1 - 12. https://doi.org/10.1016/j.landusepol.2020.105072.

YAO, Y.; MALLIK, A. U. Estimation of actual evapotranspiration and water stress in the Lijiang River Basin, China using a modified Operational Simplified Surface Energy Balance (SSEBop) model. Journal of Hydro-Environment

ISSN eletrônico 2177-2738
RA'EGA, Curitiba, PR, V.60, n.1, p. 45 – 69, 8/2024
http://dx.doi.org/10.5380/raega.v60i0.95709

Research, v. 41, 2022, p. 1–11 2022.

ZENG, N.; YOON, J.H.; MARENGO, J. A.; SUBRAMANIAM, A.; NOBRE, C. A.; MARIOTTI, A.; NEELIN, J. D. Causes and impacts of the 2005 Amazon drought. Environmental Research Letters. v. 3, 2008, p. 1 - 10. http://dx.doi.org/10.1088/1748-9326/3/1/014002.

ZHANG, H. L.; BAEYENS, J.; CÁCERES, G., DEGREVÈ, J.; LV, Y. Modular object-orient methodology for the resolution of molten salt storage tanks for CSP plants. Process in Energy and Combustion Science, vol. 53, 2016, p.1-40.